Atmos. Meas. Tech. Discuss., 6, 703–720, 2013
www.atmos-meas-tech-discuss.net/6/703/2013/
doi:10.5194/amtd-6-703-2013

Atmospheric Measurement Techniques Discussions

Measurement of motion corrected wind velocity using an aerostat lofted sonic anemometer

W. R. Stevens[1,*], W. Squier[2], W. Mitchell[2], B. K. Gullett[2], and C. Pressley[2]

[1]Oak Ridge Institute for Science and Education Postdoctoral Fellow to the US Environmental Protection Agency Office of Research and Development, National Risk Management Research Laboratory, Research Triangle Park, NC 27711, USA
[2]US Environmental Protection Agency Office of Research and Development, National Risk Management Research Laboratory, Research Triangle Park, NC 27711, USA
[*]now at: Kentucky Christian University, Dept. of Health Sciences, Grayson, KY 41143, USA

Received: 12 December 2012 – Accepted: 16 December 2012 – Published: 21 January 2013

Correspondence to: B. K. Gullett (gullett.brian@epa.gov)

Published by Copernicus Publications on behalf of the European Geosciences Union.

Abstract

An aerostat-lofted, sonic anemometer was used to determine instantaneous 3 dimensional wind velocities at altitudes relevant to fire plume dispersion modeling. An integrated GPS, inertial measurement unit, and attitude heading and reference system corrected the wind data for the rotational and translational motion of the anemometer and rotated wind vectors to a global North, West, Up coordinate system. Data were taken at rates of 10 and 20 Hz to adequately correct for motion of the aerostat. The method was applied during a prescribed forest burn. These data were averaged over 15 min intervals and used as inputs for subsequent dispersion modeling. The anemometer's orientation data are demonstrated to be robust for converting the wind vector from the internal anemometer reference system to the global reference system with an average bias between 5 and 7°. Lofted wind data are compared with sonic anemometer data acquired at 10 m on a mast located near the tether point of the aerostat and with local meteorological data.

1 Introduction

Accurate wind velocities are critical inputs for modeling atmospheric dispersion. For buoyant plumes, such as those from combustion sources, the lateral dispersion often occurs at heights well above ground based wind sensors. Additionally, local topography, nearby structures, and the localized convective forces during a fire can make ground based measurements a poor indicator of wind at higher altitudes. Currently, the de facto standard is to use meteorological models (e.g. Weather Research and Forecasting model (WRF)) or ground level meteorological data from nearby weather stations to predict plume wind velocities. However, both of these methods have uncertainties that can lead to unacceptably large errors in downwind plume position in excess of 5 km.

Attempts to determine atmospheric wind velocities beyond the reach of ground based measurements can be categorized as either in situ or remote measurements.

AMTD
6, 703–720, 2013

In situ measurements refer to wind measurements that have a fixed sampling volume located at the sensor and typically have a spatial resolution less than 1 m. In situ wind sensors are useful in determining small scale turbulence and for combining with other sensors (e.g. CO_2 and CH_4 analyzers) for information on dispersion and pollutant flux. Because the sampling volume is located at the sensor, the wind sensor itself must be lofted. Until recently, this has limited lofted in situ wind sensors to hot wire anemometers and Pitot tubes which are much less precise than sonic anemometers. Remote measurements, such as Doppler SODAR and RADAR use the reflective properties of the atmosphere to determine wind velocities. The sampling volumes of these apparatus depend upon the strength of the light or sound source and the scattering properties of the atmosphere. In both categories, attempts to determine lofted wind velocities are typically geared toward turbulence measurements and/or characterization of the Earth's boundary layer effects. As a result, these measurements are often targeted toward accurate wind magnitude measurements rather than wind directions.

Lofted in situ wind velocity and turbulence measurements have been reported by several groups (Doyle et al., 2002; Frehlich et al., 2003; Khelif et al., 1999; Lane et al., 2000; Metzger et al., 2011; Millane et al., 2010; Shuqing et al., 2004; Van den Kroonenberg et al., 2008) using winged unmanned aerial vehicles (UAVs) to discern wind velocities and turbulence. In these studies, the wind velocity vector is determined by the difference between groundspeed, determined from GPS data, and airspeed, determined from an array of pressure sensors at the nose of the vehicle. In conditions where the wind velocities are much lower than both the air and ground speeds of the UAVs, which typically have a cruising speed between 10 and 20 $m\,s^{-1}$ (Shuqing et al., 2004; Van den Kroonenberg et al., 2008), uncertainties in the calculated wind velocities can become large. Furthermore, the limited range of detectable wind direction relative to the orientation of the UAV (i.e. the UAV must fly into the wind for measurement) creates a potential for systematic error and limits the spatial resolution of the method. Kroonenberg and Martin (Van den Kroonenberg et al., 2008) have reported UAV based wind measurements with uncertainties of $\pm 1.0\,m\,s^{-1}$ (horizontal), $\pm 0.2\,m\,s^{-1}$ (vertical),

AMTD
6, 703–720, 2013

and ±20° direction (Van den Kroonenberg et al., 2008). Large uncertainties in wind direction are problematic, particularly when relying upon dispersion models to predict downwind plume trajectories. An error of 20° would correspond to a discrepancy of 1 km for every 2.7 km downwind.

A tethered aerostat provides several advantages for determining in situ wind velocities over other aerial methods. First, the aerostat motion is small compared to the minimum airspeed required for UAVs to remain aloft. This results in a smaller motion correction for the aerostat system. Additionally, since the aerostat can rotate freely around its tether, the suspended anemometer can measure a 360° range of acceptable wind directions.

There are several considerations for determining accurate wind vectors using a lofted platform. First, anemometer data must be corrected for aerostat motion and rotated so that the data are reported in a global reference system such as a North, West, Up (NWU) convention. This requires the use of a GPS unit, compass, and accelerometers. Such motion correction schemes have been applied on ships (Brooks, 2008) but this system's weight was prohibitive for an aerostat-lofted payload. Recent introduction of lightweight, integrated sensor systems capable of monitoring 3-D motion and orientation are small enough to be lofted. Furthermore, design of the mounting platform must consider stability in turbulent conditions like those found near combustion sources and minimizing effects upon the observed wind vector.

This paper describes an aerostat-lofted 3-D sonic anemometer system that corrects observed wind velocities for aerostat motion and orientation. The aerostat based sonic anemometer measurements reported here are part of an attempt to determine wind velocity data for input into plume dispersion modeling, such as from forest fires. The quality of the observed wind vector's magnitude and direction are analyzed and documented.

AMTD
6, 703–720, 2013

2 Experimental

Wind velocity measurements discussed here were part of a larger effort to characterize plume emissions from controlled forest fires. The lofted data acquisition and sampling system (DASS) has been described in detail previously (Aurell et al., 2011) Briefly, the DASS consists of an onboard PC that controls a USB-2537 data acquisition (DAQ) card (Measurement Computing; Norton MA) via USB using software generated by Labview 2010™ (National Instruments; Austin, TX). The 16 bit DAQ has 32 differential analog inputs, 24 configurable digital input/output ports, and 4 analog outputs. The sonic anemometer and an attitude heading and reference system (AHRS) were controlled by the onboard computer via RS232 ports. Power is supplied using a 52 V lithium ion polymer rechargeable battery. In addition to wind velocity data, the DASS logged CO_2 and PM concentrations in real time and volatile organic compounds and semivolatile organic compound (VOC and SVOC) sampling data. Figure 1 shows a picture of the sampling system while in flight. The DASS is lofted by a helium filled 14 ft Kingfisher™ (Aerial Products Corporation; Jacksonville, FL) aerostat with a rear sail that keeps the front of the aerostat oriented into the wind. The aerostat remains tethered to an all terrain vehicle (ATV), for the duration of the flight. The position of the aerostat sampler is changed by tether length and ATV position. The length of time that the aerostat can remain aloft is primarily determined by battery life which is determined by the number of sampling devices running and their respective power demands. The maximum height of the aerostat is determined by tether length. Currently, it is estimated that a devoted wind sensor could run at an altitude of 500 m for an entire 8 h day.

An R. M. Young 81000 sonic anemometer (R. M. Young Corp; Traverse City, Michigan) measured wind velocity along its 3 internal axes (u, v, and w) with a resolution of 0.01 $m\,s^{-1}$ and an accuracy of ±1 %. These anemometer data were recorded serially using an onboard computer. Wind data presented here were logged serially using the onboard computer. A wireless remote desktop connection to the DASS allowed for real time control and viewing of data. A flexible shaft connected the anemometer

AMTD
6, 703–720, 2013

to the bottom of the flyer approximately 1.5 m away from bottom of the aerostat. The flexible mount and relatively short distance was chosen to prevent the anemometer from getting tangled in the tether line during turbulent conditions. The orientation of the anemometer was fixed relative to the aerostat and was such that a wind velocity vector with magnitude, M, blowing parallel to the aerostat from the front to rear would be recorded as $[0, -M, 0]$ in the UVW coordinate system. The anemometer zero velocity reading was checked daily by placing a bag over the anemometer for at least 30 s.

In order to correct raw wind velocities for aerostat motion, the MTi-G (Xsens North America; Culver City, CA), a GPS-aided inertial measurement unit (IMU) with an AHRS was used. As shown in Fig. 2, the MTi-G was mounted directly onto the electronics enclosure of the sonic anemometer. The position, orientation, linear, and angular motion were recorded serially onto the onboard PC using Labview® generated software. MTi-G and anemometer data were logged asynchronously and then aligned in time after acquisition using linear interpolation.

Using the data from the MTi-G, the sonic anemometer data were corrected using the equation

$$\boldsymbol{v}_{\text{corr}} = \mathbf{R}_{GS}(\boldsymbol{v} - \boldsymbol{\Omega} \times \boldsymbol{Q}) - \boldsymbol{v}_{\text{NWU}} \quad (1)$$

Where $\boldsymbol{v}_{\text{corr}}$ is the corrected wind velocity data in NWU coordinates, $\mathbf{R}_{GS}$ is a unitless rotation matrix that when multiplied by a vector in the S (i.e. anemometer) coordinate system, the product is a vector of the same orientation in the global (i.e. NWU) coordinate system, $\boldsymbol{Q}$ is the vector describing the distance between the MTi-G (XYZ) and the anemometer origins (UVW), $\boldsymbol{\Omega}$ is the 3-D angular velocity measured by the MTi-G and $\boldsymbol{v}_{\text{NWU}}$ is the linear velocity of the sonic anemometer in NWU coordinates.

Wind velocity data were acquired on 6, 8 and 12 February 2011 at Eglin Air Force Base (Eglin AFB). Wind velocity measurements at Eglin Air Force Base (Eglin, FL) were coincident with a prescribed forest burn and were part of an effort to sample for emissions and predict pollutant dispersion downwind.

AMTD
6, 703–720, 2013

3 Results and discussion

The data presented here were taken during four flights that measured lofted wind velocities and assessed the motion and orientation correction algorithm. These data were compared with wind data simultaneously acquired at the nearby Val Paraiso meteorological station (www.ncdc.noaa.gov) that would otherwise have been used as inputs for dispersion models. At Eglin AFB, two days of flights lasted between 2 and 4 h and the aerostat height varied between 10 m and 400 m.

Figure 3 shows wind velocity, anemometer, and altitude data acquired on 12 February 2011 at Eglin AFB. The topmost trace is the aerostat altitude measured by the MTi-G, the middle plot is the vertical velocity component, and the bottom trace is a plot of the magnitude of the horizontal wind $(v_N^2 + v_W^2)^{1/2}$. Also plotted on the bottom trace are arrows that indicate the direction from which the wind is blowing. Changes in height are a result of maneuvering of the aerostat to maintain its position in the plume from the prescribed forest burn. On both Eglin AFB flights, the altitude of the aerostat was increased to match the plume height increase during the duration of the burn. The low wind speeds ($< 5\,m\,s^{-1}$) and changing wind direction in the Eglin AFB data represent unstable to slightly unstable atmospheric conditions. Figure 3b shows unsmoothed 10 Hz data acquired on 12 February 2011 to demonstrate the high temporal resolution of the motion corrected anemometer data.

Figure 4 demonstrates the reliability of the orientation correction of the MTi-G system where 0° is true North. The bottom plot contains 15 min averages motion corrected globally referenced wind vectors and the aerostat tether angle determined from the GPS coordinates of the ground tether point and the aerostat using the Haversine Eqn (Gellert, 1989). The force of the wind upon the aerostat causes the aerostat to act like a wind vane and should therefore provide a reasonable comparison to averaged wind direction data from the sonic anemometer. An average offset between the tether angle and wind velocity data was determined to be 11°, indicating good agreement. Small

AMTD
6, 703–720, 2013

discrepancies are to be expected due to the ability of the aerostat to rotate about the tether during periods of low wind.

Figure 5 demonstrates the ability of the MTi-G to quickly and reliably determine its orientation in the North-West plane despite potential interferences from onboard sampling equipment. The MTi-G uses magnetometers to determine its orientation in the North-West plane which, due to the weakness of the Earth's magnetic field, could give erroneous readings due to nearby magnetic fields from other sampling equipment on the DASS. The most likely source of magnetic interference is a semi volatile organic hydrocarbon (SVOC) sampling pump co-mounted on the aerostat for pollutant sampling. On Fig. 4, "SVOC flow rate" indicates the operating status of this pump as well as other sampling equipment. When the flow rate departs from its baseline, the sampling equipment is operating and when it remains at the baseline, this equipment is not running (the sampling equipment is triggered by CO_2 levels). The MTi-G orientation in the North-West plane is directly output from the MTi-G in the form of the r_{31} and r_{32}, terms of the $\mathbf{R}_{GS}$ rotation matrix in Eq. (1). These data were compared with handheld compass readings of the anemometer orientation logged manually every 30 s and the azimuth from the balloon to the tether point (i.e. the tether angle.) Real time aerostat tether angles were calculated from the GPS positions of the anemometer and the tether point using the Haversine Eqn (Gellert, 1989) The tether angle and anemometer orientation should agree as a result of the sail attached to the rear of the aerostat (see Fig. 1) This relationship is qualitative, however, since the aerostat is capable of rotating about the tether in low stability conditions. These rotations are observed as the spikes in the orientation data shown in Fig. 4 at times 17:33, 17:34, and 17:41 UTC. Table 1 shows the compass readings and the 10 point (1 s) average of the MTi-G orientation evaluated at the same time. The differences between these values were averaged to determine the reported average bias of 5°. The orientation values determined at 17:35 UTC were excluded from this calculation as the twisting of the balloon was noted during the measurement.

AMTD
6, 703–720, 2013

Figure 6 shows a plot of the aerostat wind velocities and altitudes averaged over 15 min with ground wind data acquired at a mast height of 10 m. The green trace represents wind data acquired from a second R. M. Young 81000 3-D sonic anemometer positioned on a 10 m mast near the tether point. These provide a direct comparison to the wind data acquired from the aerostat based anemometer. Data are not shown on 6 February 2011 due to the lack of suitable mast locations near the tether points on this day. The black arrows and points indicate wind direction and speed measured from a nearby airfield. These data were acquired from the NOAA national climactic data center (ValParaiso/Eglin Airfield, www.ncdc.noaa.gov). As expected, wind velocities measured by the aerostat are higher than the wind velocities determined by ground based anemometers. With the exception of the point at 18:00 UTC on 12 February 2011, the Airfield wind speeds are within 1 m s^{-1} of the aerostat wind speeds (both are 15-min averages). The aerostat wind directions also generally agree with the ground based anemometer and Airfield met data. However, there was a significant discrepancy between the Airfield and aerostat wind directions on 6 February 2011 of about 180°. It should be noted that the meteorological conditions on 6 February 2011 were somewhat unstable and that this discrepancy could be real. We may therefore speculate that, at least under unstable atmospheric conditions, wind data from nearby meteorological stations may not be a totally reliable proxy for the plume wind velocities.

4 Conclusions

A novel method for the measurement of 3-D wind velocities using an aerostat has been reported. Comparison with the ground compass measurements and aerostat position relative to the anchor point showed that the MTi-G's ability to correct for changes in the sonic anemometer orientation relative to the global reference system was about ±5°. Furthermore, wind data acquired from a nearby airfield agreed with local, ground based meteorological stations to within 1 m s^{-1}. For all measurements, aerostat wind speeds were higher than ground based speeds. This is likely a result of boundary layer

AMTD
6, 703–720, 2013

effects associated with the Earth's surface. Significant discrepancies were observed between the aerostat wind directions and both the ground based and nearby airfield wind directions, indicating that wind directions acquired from regional ground based meteorological stations may not sufficiently represent local conditions when precisions greater than 20 degrees are needed.

Acknowledgements. The authors would like to acknowledge support for this study from the Environmental Protection Agency (EPA) and Strategic Environmental Defense Program (SERDP). Financial support for W. R. Stevens was provided through a fellowship with the Oak Ridge Institute for Science and Education (ORISE).

References

Aurell, J., Gullett, B. K., Pressley, C., Tabor, D., and Gribble, R.: Aerostat-lofted instrument and sampling method for determination of emissions from open area sources, Chemosphere, 85, 806–811, 2011.

Brooks, I. M.: Spatially distributed measurements of platform motion for the correction of ship-based turbulent fluxes, J. Atmos. Ocean. Tech., 25, 2007–2017, 2008.

Doyle, J. D., Volkert, H., Dornbrack, A., Hoinka, K. P., and Hogan, T. F.: Aircraft measurements and numerical simulations of mountain waves over the central Alps: a pre-MAP test case, Q. J. Roy. Meteor. Soc., 128, 2175–2184, 2002.

Frehlich, R., Meillier, Y., Jensen, M. L., and Balsley, B.: Turbulence measurements with the CIRES tethered lifting system during CASES-99: calibration and spectral analysis of temperature and velocity, J. Atmos. Sci., 60, 2487–2495, 2003.

Gellert, W., Gottwald, S., Hellwich, M., Kästner, H., and Küstner, H.: The VNR Concise Encyclopedia of Mathematics, 2nd Edn., Van Nostrand Reinhold, New York, 1989.

Khelif, D., Burns, S. P., and Friehe, C. A.: Improved wind measurements on research aircraft, J. Atmos. Ocean. Tech., 16, 860–875, 1999.

Lane, T. P., Reeder, M. J., Morton, B. R., and Clark, T. L.: Observations and numerical modelling of mountain waves over the Southern Alps of New Zealand, Q. J. Roy. Meteor. Soc., 126, 2765–2788, 2000.

Metzger, S., Junkermann, W., Butterbach-Bahl, K., Schmid, H. P., and Foken, T.: Measuring the 3-D wind vector with a weight-shift microlight aircraft, Atmos. Meas. Tech., 4, 1421–1444, doi:10.5194/amt-4-1421-2011, 2011.

Millane, R. P., Stirling, G. D., Brown, R. G., Zhang, N., Lo, V. L., Enevoldson, E., and Murray, J. E.: Estimating wind velocities in mountain lee waves using sailplane flight data, J. Atmos. Ocean. Tech., 27, 147–158, 2010.

Shuqing, M., Hongbin, C., Gai, W., Yi, P., and Qiang, L.: A miniature robotic plane meteorological sounding system, Adv. Atmos. Sci., 21, 890–896, 2004.

Van den Kroonenberg, A., Martin, T., Buschmann, M., Bange, J., and Vorsmann, P.: Measuring the wind vector using the autonomous mini aerial vehicle M(2)AV, J. Atmos. Ocean. Tech., 25, 1969–1982, 2008.

AMTD
6, 703–720, 2013

Table 1. Anemometer orientation and compass values for direct comparison.

Time (HH:mm:ss)	Compass (° CCW from N)	MTiG orientation (° CCW from N)	Δ
17:33:30	100	100	0
17:34:00	35	27	8
17:34:30	10	16	6
17:35:30	10	7	3
17:36:00	5	10	5
17:36:30	10	1	9
17:37:30	15	5	10
17:38:00	10	12	2
17:38:30	20	18	2
17:39:00	23	17	6
17:39:30	25	25	0
17:40:00	32	26	6
17:40:30	15	16	1
17:41:00	10	7	3
17:41:30	8	7	1
17:42:00	2	3	1
17:42:30	8	13	5
17:43:00	8	6	2
17:43:30	2	27	25
		Average Difference:	5°

AMTD
6, 703–720, 2013

Fig. 1. Photograph of Aerostat based sampling system equipped with the 3-D anemometer mounted below the samplers.

AMTD
6, 703–720, 2013

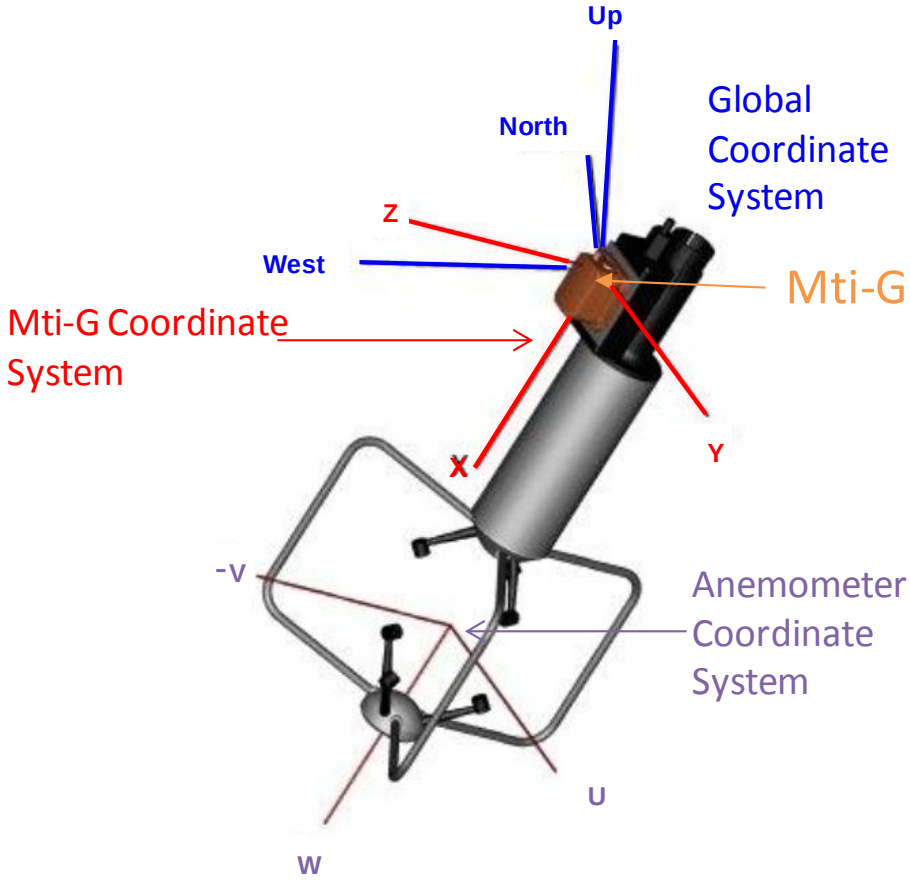

Fig. 2. Sonic Anemometer/MTi-G schematic. Note that *U* axis of the anemometer is aligned with the *Y* axis of the MTi-G, $-V$ is aligned with *Z*, and *W* is aligned with *X*. The MTi-G determines the $\mathbf{R}_{GS}$ rotation matrix to convert from the MTi-G/sonic anemometer reference frame to the North, West, Up global coordinate system.

AMTD
6, 703–720, 2013

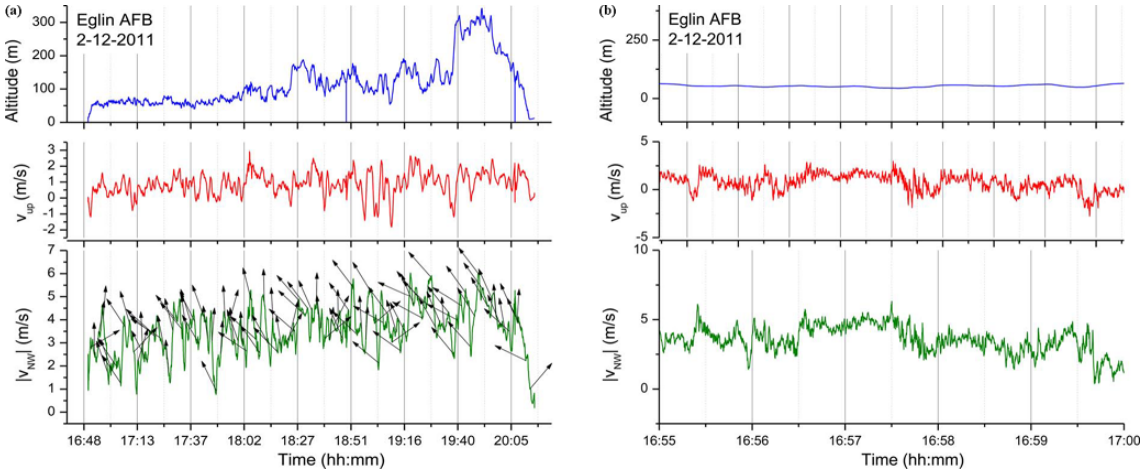

Fig. 3. Wind data from 12 February 2011. The topmost trace (blue) represents the aerostat altitude as measured by the MTi-G. The middle trace (red) is the motion corrected and rotated vertical wind velocity component. The bottom trace (green) indicates horizontal wind speed defined as $(V_N^2 + V_W^2)^{1/2}$. The black arrows in **(a)** indicate the wind direction where up is north and left is west. The data in **(a)** are smoothed using a rolling average with a window of 60 s. The data in figure **(b)** are unsmoothed 10 Hz data.

AMTD
6, 703–720, 2013

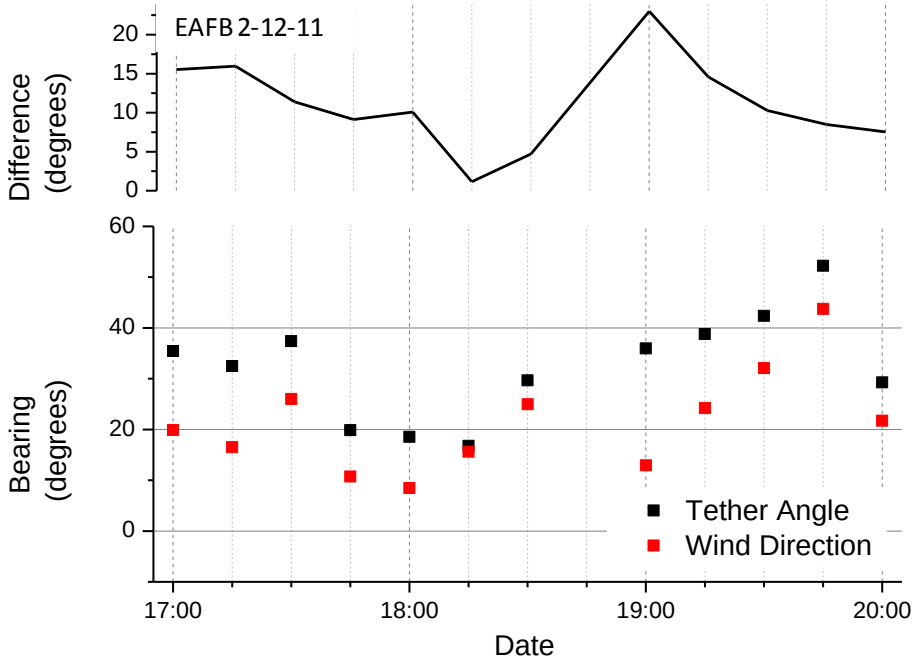

Fig. 4. Wind Direction vs. Tether Angle. Points (bottom graph) indicate 15 min averages of wind direction and tether angle where 0° corresponds to true north. The black line (top) corresponds to the difference between the average tether angle and wind direction.

AMTD
6, 703–720, 2013

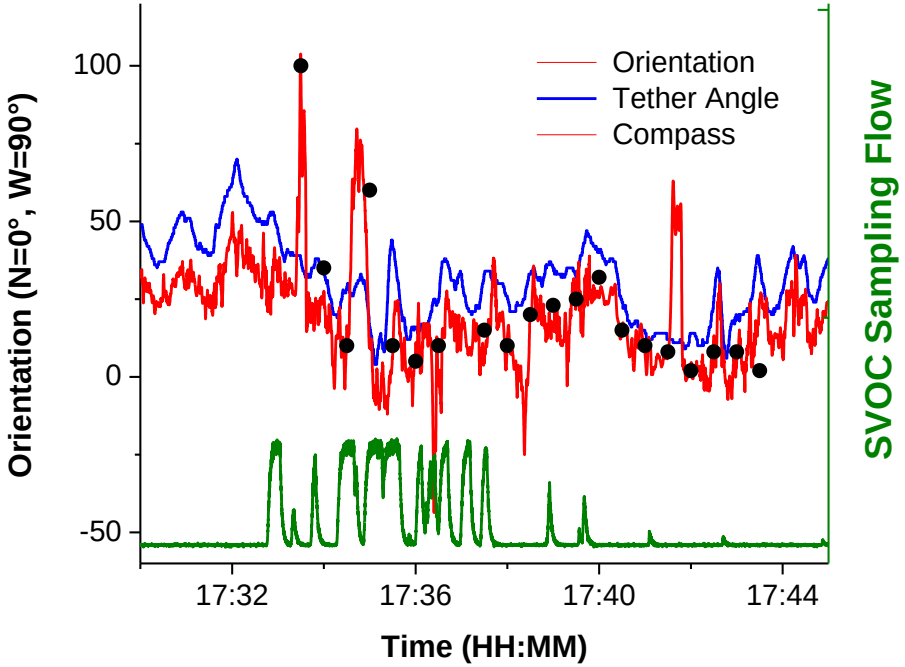

Fig. 5. Anemometer orientation (red), Aerostat tether angle (blue), plotted with compass reference points (●) where 0 corresponds to the anemometer facing north. The SVOC sampling flow rate (green) indicates the status of the onboard sampling equipment and the potential existence of transient magnetic fields which is shown to not confound the orientation measurements.

AMTD
6, 703–720, 2013

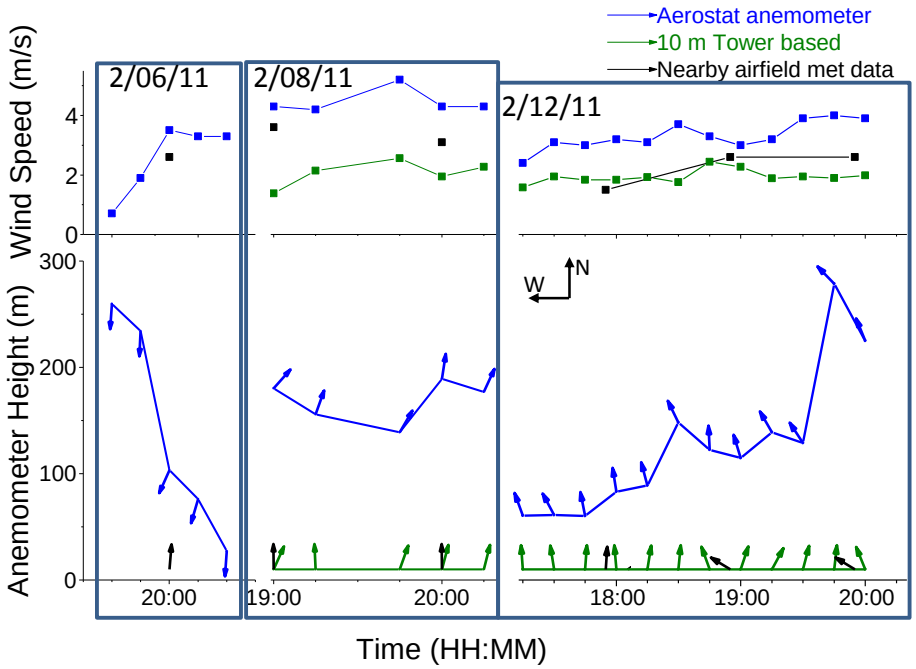

Fig. 6. Wind directions plotted at the height and time of day acquired (bottom) and magnitudes (top) observed from the Aerostat based anemometer (blue), ground 3-D sonic anemometer mounted to a 10 m tower (green), and 2-D anemometer located at a nearby airfield reported to the NOAA weather archive (black). Arrows indicate the direction from which the wind is blowing where north is up and west points to the left.

AMTD
6, 703–720, 2013